MRI Tissue Classification and Bias Field Estimation Based on Coherent Local Intensity Clustering: A Unified Energy Minimization Framework

Chunming Li[1,⋆], Chenyang Xu[2], Adam W. Anderson[1], and John C. Gore[1]

[1] Vanderbilt University Institute of Imaging Science, Nashville, TN 37232, USA
[2] Siemens Corporate Research, Princeton, NJ 08540, USA
lchunming@gmail.com

Abstract. This paper presents a new energy minimization method for simultaneous tissue classification and bias field estimation of magnetic resonance (MR) images. We first derive an important characteristic of local image intensities — the intensities of different tissues within a neighborhood form separable clusters, and the center of each cluster can be well approximated by the product of the bias within the neighborhood and a tissue-dependent constant. We then introduce a coherent local intensity clustering (CLIC) criterion function as a metric to evaluate tissue classification and bias field estimation. An integration of this metric defines an energy on a bias field, membership functions of the tissues, and the parameters that approximate the true signal from the corresponding tissues. Thus, tissue classification and bias field estimation are simultaneously achieved by minimizing this energy. The smoothness of the derived optimal bias field is ensured by the spatially coherent nature of the CLIC criterion function. As a result, no extra effort is needed to smooth the bias field in our method. Moreover, the proposed algorithm is robust to the choice of initial conditions, thereby allowing fully automatic applications. Our algorithm has been applied to high field and ultra high field MR images with promising results.

1 Introduction

Magnetic resonance imaging (MRI) is a ubiquitous and powerful medical imaging technique, which provides detailed images with high contrast between different soft tissues; MRI thus has significant advantages over other medical imaging modalities for many applications, making it especially useful for neurological, musculoskeletal, cardiovascular, and oncological imaging. However, there are commonly substantial artifacts in real MR images, such as image nonuniformities caused by inhomogeneities in the B1 or B0 fields, especially in high field (e.g. 3T) MR images. The intensity inhomogeneity may severely challenge quantitative image analysis algorithms, such as those used for image segmentation and registration. Intensity inhomogeneities are particularly severe in MRI at ultra high field strengths (e.g. 7T) and sometimes make it difficult even for expert human observers to view the images.

⋆ Corresponding author.

J.L. Prince, D.L. Pham, and K.J. Myers (Eds.): IPMI 2009, LNCS 5636, pp. 288–299, 2009.

It is commonly assumed that intensity inhomogeneities can be ascribed to a spatially varying field that is a multiplicative component of the measured image. This multiplicative component, known as a *bias field*, varies spatially because of inhomogeneities in the B0 and B1 fields. *Bias field correction* refers to a procedure to estimate the bias field from the measured image so that its effect can be eliminated. There are two main types of methods for bias correction: prospective and retrospective methods. Prospective methods aim to avoid intensity inhomogeneities in the image acquisition process. These methods, while capable of correcting intensity inhomogeneity induced by the imaging device, are not able to remove object-induced effects. In contrast, retrospective methods rely only on the information in the acquired images, and thus they can remove intensity inhomogeneities regardless of their sources. Retrospective methods include those based on filtering [1, 2, 3, 4], surface fitting [5, 6, 7, 8], histogram [9, 10], and segmentation [11, 12, 13, 14, 15, 16, 17].

Most retrospective methods assume that the bias field is smooth (i.e. slowly varying). The smoothness of the bias field is not only consistent with its physical origins in the MR imaging process, but also necessary to make the bias field correction problem tractable. However, the bias fields computed by direct implementation of most of the well-known methods are in general not smooth. This then requires an extra effort to maintain the smoothness of the computed bias field, which is often performed in an ad-hoc manner. For example, in the method of Wells *et al.* [11], an extra step of moving-average low pass filtering is introduced to smooth the computed bias field. In the method proposed by Sled *et al.* [9], the estimated bias field has to be replaced by a linear combination of smooth B-spline basis functions to generate a smooth field.

In [14], Pham and Prince proposed an energy minimization method for adaptive segmentation and estimation of the bias field. The smoothness of the bias field is ensured by adding a smoothing constraint term into the energy in their method. However, this introduces a highly computationally expensive procedure to solve a space-varying difference equation for a smooth bias field. In parametric methods (e.g. [10, 12]), which model the bias field as a linear combination of polynomial basis functions, the computed bias field is always smooth. However, such parametric methods are not able to capture bias fields that cannot be well approximated by polynomials, such as the bias field in the 7T MR images shown in Section 3.2.

Among retrospective methods, segmentation-based approaches are particularly attractive, as they unify the tasks of segmentation and bias correction into a single framework. Segmentation-based methods have been one of the most popular type of bias correction methods according to a recent review by Vovk *et al.* [18]. In these methods, segmentation and bias field estimation are interleaved to benefit each other, thereby allowing both to be refined iteratively until convergence to an optimal solution. In this process, the segmentation is usually achieved by using maximum likelihood [12, 19] or maximum a posteriori based methods [11, 13]. Fuzzy-C-Means based methods have also been used in [14, 20].

In this paper, we propose a new energy minimization method for simultaneous tissue classification and bias field estimation of MR images. We first describe an important characteristic of local image intensities — the intensities of different tissues within a neighborhood form separable clusters, and the center of each cluster can be well

approximated by the product of the bias within the neighborhood and a tissue-dependent constant. This characteristic provides an effective metric to evaluate the classification of the tissues and the estimation of the bias field in terms of a *coherent local intensity clustering (CLIC)* criterion function. This CLIC criterion is an energy on a bias field, membership functions of the tissues, and the parameters that approximate the true signal from the corresponding tissues. Tissue classification and bias field estimation are simultaneously achieved by minimizing this energy. The CLIC energy has two desirable properties: it is convex in each of its variables, which renders the proposed method robust to initialization, thereby allowing fully automatic applications; the smoothness of the derived estimate of the bias field is intrinsically ensured by the spatial coherent nature of the CLIC criterion function. As a result, no extra effort is needed for the bias field smoothing. Finally, our method is able to estimate bias fields of more general profiles, including those in high and ultra high field MR images.

2 Method

2.1 Problem Formulation

We consider the following model of MR image formation with multiplicative bias and additive noise:

$$I = bJ + n, \tag{1}$$

where I is the measured image intensity, J is the true signal to be restored, b is an unknown bias field, and n is additive noise. The goal of bias correction is to estimate the bias field b from the measured intensity I. This is obviously an underdetermined problem, as neither b nor J is known. To make the problem tractable, it is necessary to make assumptions on the unknowns b and J. The generally accepted assumption on the bias field is that it is slowly varying. Ideally, the intensity J in each tissue should take a specific value c_i of the physical property being measured (e.g. the proton density for MR images). This property, in conjunction with the spatially coherent nature of each tissue's distribution, implies that the true signal J is approximately a piecewise constant map. In addition, the additive noise n can be assumed to be zero-mean Gaussian noise.

To be specific, we assume that there are N types of tissues in the image domain Ω, and these tissues are located in N disjoint regions $\Omega_1, \cdots, \Omega_N$ in Ω. Then, the above assumptions on the true signal J and the bias field b can be formally stated as follows:

(A1) The true signal J from the i-th tissue is approximately a constant c_i, i.e. $J(\mathbf{x}) \approx c_i$ for $\mathbf{x} \in \Omega_i$. The constants $c_1, \cdots, c_N$ are assumed to be distinct from each other, as they characterize a physical property of N different tissues.

(A2) The bias field b is slowly varying in the entire image domain Ω.

Tissue classification can be achieved by partitioning the image domain Ω into N disjoint regions $\Omega_1, \cdots, \Omega_N$. Alternatively, in view of the possibility of partial volume effects, it is more advisable to perform tissue classification by seeking membership functions $u_1, \cdots, u_N$ of the tissues, which take values between 0 and 1 and satisfy

$$\sum_{i=1}^{N} u_i(\mathbf{x}) = 1, \quad \text{for all } \mathbf{x}. \tag{2}$$

The values of $u_i(\mathbf{x})$ can be interpreted as the percentage of the i-th tissue in voxel $\mathbf{x}$.

Based on the above assumptions, tissue classification and bias field estimation can be achieved by: 1) seeking the membership functions $u_1, \cdots, u_N$; 2) estimating the parameters c_i that approximate the true signal from the i-th tissue for $i = 1, \cdots, N$; 3) estimating the bias field b. In these three tasks, the membership functions $u_1, \cdots, u_N$, the parameters $c_1, \cdots, c_N$, and the bias field b can be obtained to satisfy a specified optimality criterion. For convenience, the membership functions $u_1, \cdots, u_N$ and the constants $c_1, \cdots, c_N$ are denoted by a vector valued membership function $U = (u_1, \cdots, u_N)$, and a vector $\mathbf{c} = (c_1, \cdots, c_N)$, respectively. In our proposed energy minimization framework, optimal U, $\mathbf{c}$, and b are obtained by minimizing an energy $\mathcal{F}(U, \mathbf{c}, b)$ in terms of the variables U, $\mathbf{c}$, and b.

2.2 Statistical Property of Local Intensities

The proposed algorithm is based on the properties that the bias field is slowly varying and the true signal J is piecewise approximately constant. From these basic properties, we are able to see the problem of tissue classification and bias field correction from a local viewpoint of the image intensities. These properties imply a key statistical characteristic of local intensities, which leads to an effective scheme to solve the problem of tissue classification and bias field correction.

We consider a circular neighborhood of each point $\mathbf{x} \in \Omega$, defined by $\mathcal{O}_\mathbf{x} \triangleq \{\mathbf{y} : |\mathbf{y} - \mathbf{x}| \leq \rho\}$, where ρ is the radius of the circular neighborhood. For a slowly varying bias field b, the values $b(\mathbf{y})$ for all $\mathbf{y}$ in the circular neighborhood $\mathcal{O}_\mathbf{x}$ can be well approximated by $b(\mathbf{x})$. On the other hand, the neighborhood $\mathcal{O}_\mathbf{x}$ consists of N subregions $\mathcal{O}_\mathbf{x} \cap \Omega_i$, $i = 1, \cdots, N$, where Ω_i is the region corresponding to the i-th tissue. According to the assumption (A1), the true signal J from the i-th tissue is approximately a constant c_i. Thus, the intensities $b(\mathbf{y})J(\mathbf{y})$ in each subregion $\mathcal{O}_\mathbf{x} \cap \Omega_i$ can be approximated by $b(\mathbf{x})c_i$. Thus, we have the following approximation

$$b(\mathbf{y})J(\mathbf{y}) \approx b(\mathbf{x})c_i \quad \text{for } \mathbf{y} \in \mathcal{O}_\mathbf{x} \cap \Omega_i \tag{3}$$

From the image model (1), we have

$$I(\mathbf{y}) \approx b(\mathbf{x})c_i + n(\mathbf{y}) \quad \text{for } \mathbf{y} \in \mathcal{O}_\mathbf{x} \cap \Omega_i$$

where $n(\mathbf{y})$ is additive zero-mean Gaussian noise.

The above arguments show that the measured intensities within the neighborhood $\mathcal{O}_\mathbf{x}$ can be considered as samples from N Gaussian distributions with means $b(\mathbf{x})c_i$, $i = 1, \cdots, N$. In the other words, the intensities in the neighborhood $\mathcal{O}_\mathbf{x}$ form N clusters $\{I(\mathbf{y}) : \mathbf{y} \in \mathcal{O}_\mathbf{x} \cap \Omega_i\}$, $i = 1, \cdots, N$, and the cluster center m_i of the i-th cluster can be well approximated by $m_i \approx b(\mathbf{x})c_i$. Furthermore, these clusters can be assumed to be well separated, as the cluster centers $m_i \approx b(\mathbf{x})c_i$ are distinct from each other according to the assumption (A1). This property of local intensities allows us to apply standard clustering techniques, such as K-means and fuzzy C-means algorithms, to classify the local intensities in a neighborhood into N classes.

Standard K-means or fuzzy C-means clustering are processes of minimizing a clustering criterion function. In particular, for the intensities in the neighborhood $\mathcal{O}_\mathbf{x}$, the fuzzy C-means clustering criterion function can be expressed as:

$$\mathcal{J}_{\mathbf{x}}^{\mathrm{loc}} = \int_{\mathcal{O}_{\mathbf{x}}} \sum_{i=1}^{N} u_i^q(\mathbf{y}) |I(\mathbf{y}) - m_i|^2 d\mathbf{y}, \tag{4}$$

where $q > 1$ is the fuzzifier, $u_1, \cdots, u_N$ are the membership functions satisfying $\sum_{i=1}^{N} u_i = 1$, and $m_1, \cdots, m_N$ are the cluster centers of the N clusters.

The above clustering criterion function characterizes how well the membership functions $u_1, \cdots, u_N$ give a classification of the intensities $I(\mathbf{y})$ within the neighborhood $\mathcal{O}_{\mathbf{x}}$ into N clusters or classes with cluster centers $b(\mathbf{x})c_i$. The smaller the clustering criterion function, the better the classification. Minimizing the above clustering criterion function results in an optimal set of cluster centers and membership functions as the desired classification results. However, classifying the intensities in a single neighborhood $\mathcal{O}_{\mathbf{x}}$ does not achieve our ultimate goal of bias field estimation and segmentation of the entire image. To achieve our ultimate goal, we need further development as described below.

2.3 Coherent Local Intensity Clustering

Recall that the analysis in Section 2.2 has shown that the intensities in the neighborhood $\mathcal{O}_{\mathbf{x}}$ form N separate clusters with distinct cluster centers $m_i \approx b(\mathbf{x})c_i$, $i = 1, \cdots, N$, with $c_1, \cdots, c_N$ being constants that approximate the true signal from N tissues. For the intensities $I(\mathbf{y})$ in the neighborhood $\mathcal{O}_{\mathbf{x}}$, we define a similar clustering criterion function as in Eq. (4), with the clustering centers m_i replaced by $b(\mathbf{x})c_i$. In addition, we introduce a weight for each intensity $I(\mathbf{y})$ to control its influence on the clustering criterion function. The intensity $I(\mathbf{y})$ at location $\mathbf{y}$ far away from the neighborhood center $\mathbf{x}$ should have less influence in the clustering criterion function than the locations close to $\mathbf{x}$. More specifically, we define the following clustering criterion function

$$\mathcal{J}_{\mathbf{x}}^{\mathrm{loc}}(U, \mathbf{c}, b(\mathbf{x})) \triangleq \sum_{i=1}^{N} \int_{\mathcal{O}_{\mathbf{x}}} u_i^q(\mathbf{y}) K(\mathbf{x} - \mathbf{y}) |I(\mathbf{y}) - b(\mathbf{x})c_i|^2 d\mathbf{y} \tag{5}$$

where $u_1, \cdots, u_N$ are the membership functions for N regions (tissues), and $K(\mathbf{x}-\mathbf{y})$ is the weight assigned to the intensity $I(\mathbf{y})$.

The weighting function $K(\mathbf{x}-\mathbf{y})$ is preferably designed so that its value decreases as the distance from $\mathbf{y}$ to the neighborhood center $\mathbf{x}$ increases. In this paper, the weighting function K is chosen as a truncated Gaussian kernel

$$K(\mathbf{u}) = \begin{cases} \frac{1}{a} e^{-|\mathbf{u}|^2/2\sigma^2} & \text{for } |\mathbf{u}| \le \rho; \\ 0 & \text{else,} \end{cases} \tag{6}$$

With such a truncated Gaussian kernel $K(\mathbf{x}-\mathbf{y})$, the above clustering criterion function $\mathcal{J}_{\mathbf{x}}^{\mathrm{loc}}$ can be written as

$$\mathcal{J}_{\mathbf{x}}^{\mathrm{loc}}(U, \mathbf{c}, b(\mathbf{x})) = \sum_{i=1}^{N} \int u_i^q(\mathbf{y}) K(\mathbf{x} - \mathbf{y}) |I(\mathbf{y}) - b(\mathbf{x})c_i|^2 d\mathbf{y} \tag{7}$$

as $K(\mathbf{x} - \mathbf{y}) = 0$ for $\mathbf{y} \notin \mathcal{O}_{\mathbf{x}}$.

The above clustering criterion characterizes the local performance of the tissue classification associated with the membership functions $u_1, \cdots, u_N$, which are defined on the entire image domain. The desired tissue classification on the entire image domain should have good local performance in terms of the above clustering criterion for every neighborhood $\mathcal{O}_{\mathbf{x}}$. Therefore, we seek the membership function U, constant $\mathbf{c}$, and bias field b such that $\mathcal{J}_{\mathbf{x}}^{\mathrm{loc}}(U, \mathbf{c}, b(\mathbf{x}))$ is minimized for all $\mathbf{x} \in \Omega$.

We have defined the above local clustering criterion function $\mathcal{J}_{\mathbf{x}}^{\mathrm{loc}}$ based on the smoothness of the bias field b. The definition of such local clustering criterion function $\mathcal{J}_{\mathbf{x}}^{\mathrm{loc}}$ intrinsically implies the smoothness of the optimal field estimator b that minimizes $\mathcal{J}_{\mathbf{x}}^{\mathrm{loc}}$ for all $\mathbf{x} \in \Omega$. The optimal field b is denoted by $\hat{b}$. The smoothness of $\hat{b}$ can be intuitively explained as follows. The clustering criterion function $\mathcal{J}_{\mathbf{x}}^{\mathrm{loc}}$ involves all the intensities $I(\mathbf{y})$ in the neighborhood $\mathcal{O}_{\mathbf{x}}$. Therefore, the value of $b(\mathbf{x})$ that minimizes $\mathcal{J}_{\mathbf{x}}^{\mathrm{loc}}$ depends on all the intensities $I(\mathbf{y})$ in the neighborhood $\mathcal{O}_{\mathbf{x}}$. As the neighborhood center moves from $\mathbf{x}$ to a point $\mathbf{x}' = \mathbf{x} + \Delta\mathbf{x}$ for a small displacement $\Delta\mathbf{x}$, the majority of points in the neighborhood $\mathcal{O}_{\mathbf{x}}$ remain in the neighborhood $\mathcal{O}_{\mathbf{x}'}$. Therefore, the value of $\hat{b}(\mathbf{x}')$ is close to $\hat{b}(\mathbf{x})$, which indicates the smoothness of $\hat{b}$. The smoothness of the optimal bias field estimator $\hat{b}$ will be clearly seen from its closed form solution in Section 2.4.

The above argument shows the spatial coherence of the minimization of the local clustering criterion $\mathcal{J}_{\mathbf{x}}^{\mathrm{loc}}$ for all $\mathbf{x} \in \Omega$ — the local clustering criterion functions $\mathcal{J}_{\mathbf{x}}^{\mathrm{loc}}$ for different $\mathbf{x}$ are not minimized independently. There is a strong relationship between the local clustering criterion functions $\mathcal{J}_{\mathbf{x}}^{\mathrm{loc}}$ for neighboring points $\mathbf{x}$ and the corresponding results of minimization, due to the overlap of the neighborhoods. Therefore, we call the minimization of the local clustering criterion functions $\mathcal{J}_{\mathbf{x}}^{\mathrm{loc}}$ for all $\mathbf{x} \in \Omega$ a process of *coherent local intensity clustering (CLIC)*.

Minimization of $\mathcal{J}_{\mathbf{x}}^{\mathrm{loc}}$ for all $\mathbf{x} \in \Omega$ can be achieved by minimizing the integral of $\mathcal{J}_{\mathbf{x}}^{\mathrm{loc}}$ over Ω. Therefore, we define an energy $\mathcal{J}(U, \mathbf{c}, b) \triangleq \int \mathcal{J}_{\mathbf{x}}^{\mathrm{loc}}(U, \mathbf{c}, b(\mathbf{x}))d\mathbf{x}$, i.e.

$$\mathcal{J}(U, \mathbf{c}, b) \triangleq \int \sum_{i=1}^{N} \int u_i^q(\mathbf{y}) K(\mathbf{x} - \mathbf{y}) |I(\mathbf{y}) - b(\mathbf{x})c_i|^2 d\mathbf{y} d\mathbf{x} \tag{8}$$

By changing the order of integration, the above energy $\mathcal{J}(U, \mathbf{c}, b)$ can be written in the form:

$$\mathcal{J}(U, \mathbf{c}, b) = \int \sum_{i=1}^{N} u_i^q(\mathbf{y}) d_i(I(\mathbf{y})) d\mathbf{y} \tag{9}$$

where

$$d_i(I(\mathbf{y})) \triangleq \int K(\mathbf{x} - \mathbf{y}) |I(\mathbf{y}) - b(\mathbf{x})c_i|^2 d\mathbf{x} \tag{10}$$

The minimization of the energy $\mathcal{J}(U, \mathbf{c}, b)$ is subject to the constraint

$$\sum_{i=1}^{N} u_i = 1.$$

The minimization of the above energy $\mathcal{J}(U, \mathbf{c}, b)$ is described in Section 2.4. The algorithm for minimizing this energy is simply referred to as the *coherent local intensity*

clustering (CLIC) algorithm. The estimated bias field and true signal are given by $\hat{b}$, and $I/\hat{b}$, respectively. We note that the proposed method can provide a solution only up to a scaling factor. In fact, for any bias field $\hat{b}$ and vector $\hat{\mathbf{c}}$ that minimize the energy $\mathcal{J}(U, \mathbf{c}, b)$, the bias field $s\hat{b}$ and vector $\hat{\mathbf{c}}/s$ for any constant s also minimize the energy.

2.4 Energy Minimization

The energy $\mathcal{J}(U, \mathbf{c}, b)$ is convex in each of its variables. Therefore, there is a unique minimizer of the energy $\mathcal{J}(U, \mathbf{c}, b)$ in each variable, given the other two variables remain fixed. Thus, minimization of the energy $\mathcal{J}(U, \mathbf{c}, b)$ can be performed by an interleaving process of minimization with respect to the variables U, $\mathbf{c}$, and b. Moreover, the energy minimization algorithm is robust to the initialization of the variables U, $\mathbf{c}$, and b.

For the case $q > 1$, the above constrained energy minimization results in a fuzzy membership function $\hat{u}_1, \cdots, \hat{u}_N$, which take values between 0 and 1, yielding a result of *soft segmentation*. For the case $q = 1$, the constrained energy minimization results in binary maps $\hat{u}_1, \cdots, \hat{u}_N$, with values being either 0 or 1, yielding a result of *hard segmentation*. The segmentation results can be visualized by showing the image $\sum_{i=1}^{N} \hat{c}_i \hat{u}_i$.

2.5 Minimization with Respect to Variables c and b

For any $q \geq 1$, the solutions to the minimization of the energy $\mathcal{J}(U, \mathbf{c}, b)$ with respect to the variables $\mathbf{c}$ and b are given as below:

- For fixed U and b, there is a unique minimizer of the energy $\mathcal{J}(U, \mathbf{c}, b)$ with respect to $\mathbf{c}$, denoted by $\hat{\mathbf{c}} = (\hat{c}_1, \cdots, \hat{c}_N)$. It can be shown that

$$\hat{c}_i = \frac{\int (b * K) I u_i^q d\mathbf{x}}{\int (b^2 * K) u_i^q d\mathbf{x}}, \quad i = 1, \cdots, N. \tag{11}$$

  where $*$ is the convolution operation.
- Given U and $\mathbf{c}$, there is a unique minimizer of the energy $\mathcal{J}(U, \mathbf{c}, b)$ with respect to b, denoted by $\hat{b}$. It can be shown that

$$\hat{b} = \frac{(IJ^{(1)}) * K}{J^{(2)} * K} \tag{12}$$

  where $J^{(1)} = \sum_{i=1}^{N} c_i u_i^q$ and $J^{(2)} = \sum_{i=1}^{N} c_i^2 u_i^q$.

Note that the convolutions with a kernel K in the expression of $\hat{b}$ in Eq. (12) confirms the smoothness of the derived optimal bias field $\hat{b}$, which has been explained from the definition of the clustering criterion function $\mathcal{J}_{\mathbf{x}}^{\text{loc}}$ in the previous section.

2.6 Minimization with Respect to the Membership Function U

The minimization of $\mathcal{J}(U, \mathbf{c}, b)$ with respect to the membership function U should be considered for the cases of $q > 1$ and $q = 1$ separately, which correspond to soft

segmentation and hard segmentation, respectively. We first consider the case $q > 1$. For fixed $\mathbf{c}$ and b, there is a unique minimizer of the energy $\mathcal{J}(U, \mathbf{c}, b)$ with respect to U. We denote this minimizer by $\hat{U} = (\hat{u}_1, \cdots, \hat{u}_N)$. It can be shown that

$$\hat{u}_i(\mathbf{y}) = \frac{1}{\sum_{k=1}^{N} \left(\frac{d_i(I(\mathbf{y}))}{d_k(I(\mathbf{y}))} \right)^{\frac{1}{q-1}}} \tag{13}$$

For the case of $q = 1$, given the variables $\mathbf{c}$ and b fixed, the energy $\mathcal{J}(U, \mathbf{c}, b)$ is minimized when $U = \hat{U} = (\hat{u}_1, \cdots, \hat{u}_N)$ as below:

$$\hat{u}_i(\mathbf{x}) = \begin{cases} 1, \, i = i_{\min}(\mathbf{x}); \\ 0, \, i \neq i_{\min}(\mathbf{x}). \end{cases} \tag{14}$$

where

$$i_{\min}(\mathbf{x}) = \arg\min_i \{d_i(I(\mathbf{x}))\}.$$

3 Experimental Results

In this section, we apply the proposed CLIC algorithm to 3T and 7T MR images to demonstrate its effectiveness. As mentioned above, the CLIC algorithm is robust to initialization of the variables U, $\mathbf{c}$, and b. To demonstrate the robustness, the initializations of these variables for the experiments in this paper are all generated as random numbers (for $\mathbf{c}$) and random fields (for b and U). The parameter σ in the truncated Gaussian kernel K can be chosen from the range of $4 \leq \sigma \leq 7$ for 3T MR images, while we set $\sigma = 4$ for 7T MR images. The fuzzifier q is set to 2 for all the images in this paper.

3.1 Application to 3T MR Images

We first show the results for MR images obtained at 3T in Fig. 1. Inhomogeneity of the image intensity can be clearly seen in the original images in Fig. 1(a). The extracted bias field and the corresponding bias corrected image are shown in Figs 1(b) and 1(c), respectively. Note that we usually display the extracted bias field only on a mask of the brain. In the bias corrected image, the intensities within each tissue become quite homogeneous.

The improvement of the image quality in terms of intensity homogeneity can also be demonstrated by comparing the histograms of the original images and the bias corrected images, as shown in Fig. 1(f). There are three well-defined and well-separated peaks in the histograms of the bias corrected image, corresponding to the background, gray matter (GM), and white matter (WM). The peak for the cerebrospinal fluid (CSF) is not so well-defined (the one between the peaks for the background and the GM), as the volume of the CSF is relatively small. The histograms of the original images do not have such well-separated or well-defined peaks due to the mixture of the intensity distributions for different tissues caused by the bias.

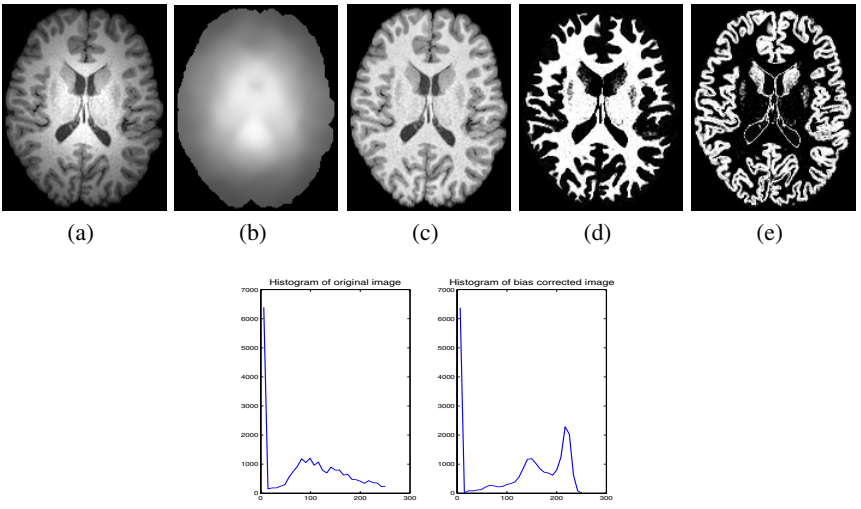

Fig. 1. Applications of our method to a 3T MR image. (a) Original image; (b) Extracted bias field (displayed on the brain mask); (c) Bias corrected image; (d) Membership function for WM; (e) Membership function for GM; (f) Comparison of histograms of the original image (left) and bias corrected image (right).

It is worth noting that the proposed algorithm does not rely on skull stripping. For example, we apply the CLIC algorithm to a 3T MR image of a brain shown in Fig. 2(a) without stripping the skull. Desirable results of bias corrected image and tissue segmentation are obtained as shown in Figs. 2(b) and 2(c), respectively. Comparison of the histograms of the original images in Fig. 2(d) further demonstrates the improved image quality.

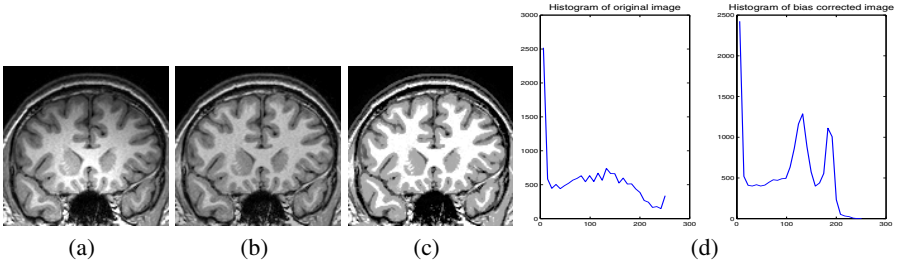

Fig. 2. Applications of our method to a 3T MR image. (a) Original image; (b) Bias corrected image; (c) Segmentation result; (d) Comparison of histograms of the original image (left) and bias corrected image (right).

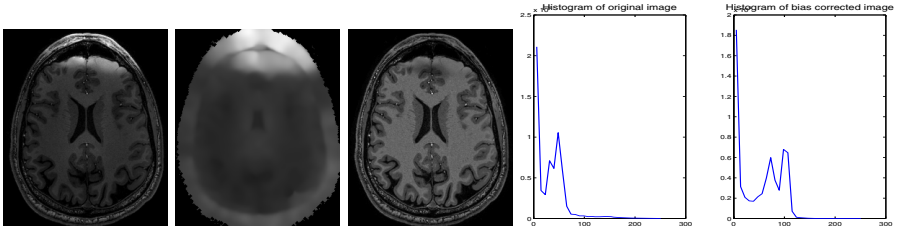

Fig. 3. Applications of our method to a 7T MR image. (a) Original image; (b) Extracted bias field (displayed on the brain mask); (c) Bias corrected image; (d) Comparison of histograms of the original image (left) and bias corrected image (right).

3.2 Application to 7T MR Images

The CLIC algorithm has also been tested on 7T MR images, where attenuation of the RF fields and standing wave effects are more pronounced than at lower fields. In addition, susceptibility-induced gradients, which scale with the main field, cause signal dephasing and more local signal bias. Such effects are most pronounced at air/tissue interfaces, as can be seen from the 7T MR image in Fig. 3(a), which appear as highly localized and strong biases. The extracted bias field of this image and the bias corrected image are shown in Figs. 3(b) and 3(c), respectively. Comparison of the histograms of the original image (left in Fig. 3(d)) and the bias corrected image (left in Fig. 3(d)) further demonstrates the improved image quality after bias field correction.

3.3 Validation and Method Comparisons

To quantitatively evaluate and compare the proposed CLIC algorithm with other algorithms. we use the synthetic MR images with ground truth from BrainWeb: `http://www.bic.mni.mcgill.ca/brainweb/`. We use Jaccard similarity (JS) as the metric to quantitatively evaluate the segmentation accuracy. The JS is defined as

$$J(S_1, S_2) = \frac{|S_1 \cap S_2|}{|S_1 \cup S_2|} \tag{15}$$

Table 1. Evaluation of tissue segmentation in terms of Jaccard Similarity Coefficients

		Wells	Leemput	**CLIC**
Synthetic image 1	WM	90.60%	85.17%	**95.76**%
	GM	80.90%	71.12%	**88.37**%
	CSF	84.53%	81.38%	**89.87**%
Synthetic image 2	WM	91.05%	82.30%	**92.55**%
	GM	80.02%	65.37%	**82.19** %
	CSF	82.49%	79.07%	**86.33** %

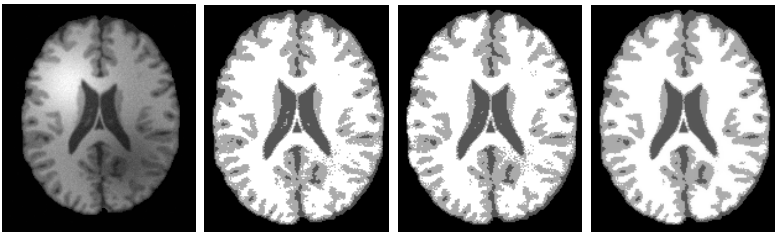

(a) (b) (c) (d)

Fig. 4. Segmentation results for a synthetic image. (a) Original image; (b) Result of Wells *et al.*'s method. (c) Result of Leemput *et al.*'s method. (d) Result of our method.

where $|\cdot|$ represents the area of a region, S_1 is the region segmented by the algorithm, and S_2 is the corresponding region in the ground truth. The closer the JS values to 1, the better the segmentation and bias correction. We applied the algorithms of Wells *et al.* [11] and Leemput *et al.* [12] on two synthetic images. The tissue segmentation for the noisy images is shown in Fig. 4 as an example. The resulting JS values for the three methods are listed in Table 1. It can be seen that the JS values of our method are higher than the other two methods.

4 Conclusion

We have introduced a coherent local intensity clustering (CLIC) criterion function as a metric to evaluate tissue classification and bias field estimation based on an important characteristic of local intensities in MR images. An integration of this metric defines an energy on a bias field, membership functions of the tissues, and the parameters that approximate the true signal from the corresponding tissues. Tissue classification and bias field estimation are simultaneously achieved by minimizing this energy. The smoothness of the derived optimal bias field is intrinsically ensured by the spatially coherent nature of the CLIC criterion function. As a result, no extra effort is needed to smooth the bias field in our method. Moreover, the proposed CLIC algorithm is robust to the choice of initial conditions, thereby allowing fully automatic applications. The CLIC algorithm has been applied to high field and ultra high field MR images with promising results.

References

1. Lewis, E., Fox, N.: Correction of differential intensity inhomogeneity in longitudinal MR images. Neuroimage 23(1), 75–83 (2004)
2. Johnston, B., Atkins, M.S., Mackiewich, B., Anderson, M.: Segmentation of multiple sclerosis lesions in intensity corrected multispectral MRI. IEEE Trans. Med. Imag. 15(2), 154–169 (1996)

3. Brinkmann, B., Manduca, A., Robb, R.: Optimized homomorphic unsharp masking for MR grayscale inhomogeneity correction. IEEE Trans. Med. Imag. 17(2), 161–174 (1998)
4. Cohen, M., DuBois, R., Zeineh, M.: Rapid and effective correction of RF inhomogeneity for high field magnetic resonance imaging. Hum. Brain Mapp. 10, 204–211 (2000)
5. Vokurka, E., Thacker, N., Jackson, A.: A fast model independent method for automatic correction of intensity nonuniformity in MRI data. J. Magn. Reson. Imag. 10, 550–562 (1999)
6. Meyer, C., Bland, P., Pipe, J.: Retrospective correction of intensity inhomogeneities in MRI. IEEE Trans. Med. Imag. 14(1), 36–41 (1995)
7. Milles, J., Zhu, Y.M., Chen, N., Panych, L.P., Gimenez, G., Guttmann, C.R.: MRI intensity nonuniformity correction using simultaneously spatial and gray-level histogram information. In: Proc. SPIE Med. Imag. 2004: Physiol., Function, Structure Med. Images, vol. 5370, pp. 734–742 (2004)
8. Vemuri, P., Kholmovski, E., Parker, D., Chapman, B.: Coil sensitivity estimation for optimal SNR reconstruction and intensity inhomogeneity correction in phased array MR imaging. In: Christensen, G.E., Sonka, M. (eds.) IPMI 2005. LNCS, vol. 3565, pp. 603–614. Springer, Heidelberg (2005)
9. Sled, J., Zijdenbos, A., Evans, A.: A nonparametric method for automatic correction of intensity nonuniformity in MRI data. IEEE Trans. Med. Imaging 17(1), 87–97 (1998)
10. Styner, M., Brechbuhler, C., Szekely, G., Gerig, G.: Parametric estimate of intensity inhomogeneities applied to MRI. IEEE Trans. Med. Imag. 19(3), 153–165 (2000)
11. Wells, W., Grimson, E., Kikinis, R., Jolesz, F.: Adaptive segmentation of MRI data. IEEE Trans. Med. Imag. 15(4), 429–442 (1996)
12. Leemput, V., Maes, K., Vandermeulen, D., Suetens, P.: Automated model-based bias field correction of MR images of the brain. IEEE Trans. Med. Imag. 18(10), 885–896 (1999)
13. Guillemaud, R., Brady, J.: Estimating the bias field of MR images. IEEE Trans. Med. Imag. 16(3), 238–251 (1997)
14. Pham, D., Prince, J.: Adaptive fuzzy segmentation of magnetic resonance images. IEEE Trans. Med. Imag. 18(9), 737–752 (1999)
15. Zhang, Y., Brady, M., Smith, S.: Segmentation of brain MR images through a hidden Markov random field model and the expectation-maximization algorithm. IEEE Trans. Med. Imag. 20(1), 45–57 (2001)
16. Liew, A., Yan, H.: An adaptive spatial fuzzy clustering algorithm for 3-D MR image segmentation. IEEE Trans. Med. Imag. 22(9), 1063–1075 (2003)
17. Li, C., Gatenby, C., Wang, L., Gore, J.: A robust parametric method for bias field estimation and segmentation of MR images. In: Proceedings of IEEE Conference on Computer Vision and Pattern Recognition (CVPR) (2009)
18. Vovk, U., Pernus, F., Likar, B.: A review of methods for correction of intensity inhomogeneity in MRI. IEEE Trans. Med. Imag. 26(3), 405–421 (2007)
19. Gispert, J., Reig, S., Pascau, J., Vaquero, J., Garcia-Barreno, P., Desco, M.: Method for bias field correction of brain t1-weighted magnetic resonance images minimizing segmentation error. Human Brain Mapping 22(2), 133–144 (2004)
20. Ahmed, M., Yamany, S., Mohamed, N., Farag, A., Moriarty, T.: A modified fuzzy c-means algorithm for bias field estimation and segmentation of MRI data. IEEE Trans. Med. Imaging 21(3), 193–199 (2002)